

# Mass and Stiffness Matrices and Frequencies of Simple Beam Elements Based on Real Shape Functions

**Pedram Abouzari, Karen Khanlari \***

Department of Civil Engineering, Faculty of Civil & Earth Resources Engineering, Central Tehran Branch, Islamic Azad University, Tehran, Iran  
Email: ped.abouzari.eng@iauctb.ac.ir, karkhanlari@gmail.com, kar.khanlari@iauctb.ac.ir

\*Corresponding author

**Reza Esmaeelabadi**

Department of Civil Engineering, Roudehen Branch, Islamic Azad University, Roudehen, Iran  
Email: esmaeilabadi@riau.ac.ir

**Received: 25 January 2022, Revised: 9 April 2022, Accepted: 15 April 2022**

**Abstract:** In this research, we investigate and compare the natural frequencies of simple beams and their mass and stiffness matrices of the two methods: classic shape functions and real shape functions. To this end, we solve the beam motion Equation and apply boundary conditions. This article shows that the coefficients of the real shape functions, and consequently, the real shape functions, become harmonic and hyperbolic and also, they are dependent on the natural frequency value of the element. As a result, the real mass and the real stiffness matrix of each element are also dependent on the element frequency. The frequency values obtained from these two methods are compared with the exact frequency values of two simple beam types with different support conditions. In this way, we determine which method leads to more accurate and acceptable frequencies for these beams. Based on the obtained results, the percentage of frequency error obtained by the classical method is relatively high in the sample beams. Hence, the natural frequency value of the beams studied using exact shape functions shows a small error compared to the classical method in terms of the exact frequency value of these beams. It is of note that the frequency error obtained from the classical method is greater in the elements with a higher natural frequency. Overall, obtaining the exact natural frequency of an element will result in accurate dynamic responses and more appropriate analyses and designs.

**Keywords:** Beam Element, High Natural Frequency, Mass and Stiffness Matrices, Real and Classic Shape Functions

**How to cite this paper:** Pedram Abouzari, Karen Khanlari, and Reza Esmaeelabadi, “Mass and Stiffness Matrices and Frequencies of Simple Beam Elements Based on Real Shape Functions”, Int J of Advanced Design and Manufacturing Technology, Vol. 15/No. 2, 2022, pp. 83–96. DOI: 10.30495/admt.2022.1949656.1336.

**Biographical notes:** **Pedram Abouzari** is a Ph.D. Candidate in Structural Civil Engineering of the Department of Civil Engineering, Central Tehran Branch, Islamic Azad University, Tehran, Iran. He received his M.Sc. in Structural Civil Engineering from IAU, Central Tehran Branch, Tehran, Iran in 2015. **Karen Khanlari** is an assistant professor and faculty member of the Department of Civil Engineering at Central Tehran Branch, Islamic Azad University, Tehran, Iran. He received his Ph.D. in Structural Civil Engineering from IAU, Science and Research branch, Tehran, Iran in 2006. **Reza Esmaeelabadi** is an assistant professor and faculty member of the Department of Civil Engineering at Roudehen Branch, Islamic Azad University, Roudehen, Iran. He received his Ph.D. in Structural Civil Engineering from IAU, Science and Research branch, Tehran, Iran in 2017.

---

## 1 INTRODUCTION

---

Since the emergence of structural science, one of the most important concerns of engineers, experts, and researchers in designing, analyzing, and constructing structures has been upgrading resistance and safety to natural and man-made disasters to protect human lives and property. It is possible to achieve accuracy and quality in the steps mentioned above. A structure itself is composed of a set of smaller elements (e.g., beams, columns, and plates) with different loading, frequency, analysis, and design methods. These elements complement one structure, and the failure of one of these components can affect the other elements. Observing psychological safety of people residing in a structure requires creating a safer structure in which all elements are carefully analyzed, designed, and executed. Each element can achieve a more accurate dynamic response by obtaining more exact shape functions and, consequently, more accurate natural frequencies. In this study, we investigate and compare the natural frequency values of a simple beam with a high-frequency element under different support conditions based on simple and real shape functions. We also introduce some other elements of high natural frequency obtained by experimental or theoretical research.

In a study on the free vibrations of reinforced sheets, Rahbar and Abdollah [1] investigated the vibrations of rectangular reinforced sheets. The main purpose of the paper is to investigate the various functions that describe the shape of sheet modes reinforced in ship structures. In the following, they have introduced the geometrical properties, modeled by ANSYS software, of the reinforcing sheets of a bulk ship. The natural frequency of its first mode is about 50 Hz and has shown that with increasing sheet length, the natural frequencies of the dominant modes decrease. Azimi-Zawareie [2] has done a detailed dynamic analysis of truss structures, and has obtained the vibrational properties of truss-like structures using classical formulations for a truss element based on an inaccurate, and sometimes inadequate, linear displacement function in a number of frequencies and shapes of vibrational states, which can be seen in the reference. In this study, these glitches were resolved by using a precise element formulation methodology that utilizes the precise displacement function of the elements.

Rana [3] has studied the dynamic analysis of the fixed-end beams in theoretical and experimental methods and compared their results with each other. The beams investigated by the features mentioned in this paper show a significant natural frequency of about 70 Hz for dominant modes. Satpathy and Dash [4] carried out research on the dynamic analysis of the cantilever beam. First, the Equation of motion of this beam is formulated

and its natural frequencies are obtained using ANSYS software and experimental method. This beam also has a high natural frequency. Sawant [5] studies the vibrations of a free beam in both theoretical and experimental methods. The investigated model of the beam is assumed to be linear and all properties along the beam are the same. The steel beam is thin, its dimensions are on millimeter scale, and its other characteristics have been clearly mentioned in the reference. These types of beams can be considered as part of the high frequency elements due to their natural frequency value.

Tatar [6] defines the dynamic behavior of a frame with conical members and obtains and compares the eigenvalues and natural frequencies of its modes using the finite element method and experiment. The geometrical properties of this frame are mentioned in this research. The natural frequency of this frame is high. AL and Kumawat [7] have investigated the natural frequencies of aluminum beams. The effect of crack formation on the natural frequency value of the beam is tested in their paper. The beam models studied also have a relatively high natural frequency. Chao and Dong [8] have investigated the natural frequency of an integrated beam and a joint beam with a shear connection in which both beams have been hammered by vibration. The natural frequency of the dominant modes of both beams indicates that the frequency of the integrated beam is greater in all modes than the joint beam, and both are high frequency values. Delhez [9] has studied the modal analysis of pre-stressed steel strip in numerical and experimental methods and compared the natural frequency value in two ways. Model specifications and experimental conditions are fully described in their paper. The pre-stressed steel strip has a high natural frequency. Esfandiari et al. [10] examined the natural frequency of the concrete beam model. In their paper, natural frequencies of normal concrete beams and those with different failure rates and loads are investigated and compared. This type of beam also has a high natural frequency. Beams that have been loaded or damaged have a lower natural frequency.

Gandomkar et al. [11] have investigated the frequency profile of a composite steel plate profile system with a board. These panels are used as a flooring system and the purpose of obtaining their frequency range is to determine whether they are suitable for human use or not. The physical characteristics of the models, the thickness, and distance of the screws are fully stated in the reference.

Joubaneh et al. [12] investigated the vibration of sandwich beams with different boundary conditions. The geometrical parameters and characteristics of the beams are given in their article. The natural frequencies of these beams were obtained and compared with analytical and experimental methods under several

boundary conditions, geometries, and different physical properties. According to the study, these types of beams also showed a naturally high frequency. Other high frequency elements include a composite beam. Composite materials are used in many industrial and commercial aspects such as aircraft, ships, vehicles, etc. In an article by Krishnaraju et al. [13], a sample composite beam made of natural fiber was tested and its natural frequency was measured. Test conditions and sample specifications are stated in the reference.

Trišović [14] analyzed the dynamic behavior of an electric motor shaft. Shaft modeling is considered as a beam element. The natural frequency values of the first few modes are obtained and have a high frequency. One of the best ways to detect a fault in a system is to check the natural frequencies of the system, which can be easily and accurately measured. This method is used for simple and failure elements that can be modeled theoretically. Yang et al. [15] investigated the frequency value for cracked or failed beam elements. This paper examines the theory of failure detection by the beam element frequency method.

As a result of this research, it was found that by increasing partial crack length, the rate of first mode frequency increases. In [16], an efficient and scalable approach was introduced for simulating inhomogeneous and non-linear elastic objects. In this work, the applied numerical coarsening approach consists of optimizing non-conforming and matrix-valued shape functions to allow for predictive simulation of heterogeneous materials with non-linear constitutive laws, even on coarse grids. Hence, it allows saving orders of magnitude in computational time compared to traditional finite element computations. Also, in this work, crucial geometric and physical properties such as the partition of unity and exact reproduction of representative fine displacements were considered to avoid using discontinuous Galerkin methods. The results showed that this method could simulate inhomogeneous and non-linear materials (with no parameter tuning) significantly better than previous approaches that homogenize the constitutive model.

In [17], a new model based on the Finite Element (FE) model and real healthy state was presented for damage detection of mechanical systems in the presence of uncertainties such as modeling errors, measurement errors, varying loading conditions, and environmental noises. Another point to consider in this paper is designing a developed Deep Convolutional Neural Network (DCNN) with training interference and customized architecture to learn the features. In addition, the proposed DCNN was trained using raw frequency data of the FE model and real healthy state and finally tested using the raw frequency data of the real system. The proposed DCNN could directly learn the features from raw frequency data of the FE model and

real healthy state. As a result, it could discover the damage-sensitive features for damage detection of a real system. In this method, only dynamic responses of a real healthy system were used to update the FE model and minimize errors. The efficiency of the proposed method was validated using the experimental beam structure. Time data, several manual features from time and frequency data, and two intelligent methods were used as comparison criteria. The results revealed that the proposed method can learn the features from raw frequency data and achieve higher accuracy than other comparative methods.

Adhikari et al. [18] investigated the Free and forced bending vibration of damped nonlocal nano-beams resting on an elastic foundation. In this article, two types of nonlocal damping models, namely, strain-rate-dependent viscous damping and velocity-dependent viscous damping have considered. They have developed a frequency-dependent dynamic finite element method to obtain the forced vibration response. Also, in this work frequency-adaptive complex-valued shape functions have used for the derivation of the dynamic stiffness matrix. It is shown that there are six unique coefficients which define the general dynamic stiffness matrix. It is proved that the general dynamic stiffness matrix reduces to the well-known special cases under different conditions. The stiffness and mass matrices of the nonlocal beam has been achieved using the conventional finite element method. Then, The Results from the dynamic finite element method and the conventional finite element method have been compared. Explicit closed-form expressions of the dynamic response for both the cases have been obtained and the role of crucial system parameters such as, the damping factors, the nonlocal parameter and the foundation stiffness have been investigated.

In a study by Corrêa et al. [19] the focus has been applied on the G/XFEM for free vibration analysis of thin and thick curved beam models. In this research the accuracy of frequencies values, the convergence to reach them, and the frequency spectrum are some of the points it has been discussed. Also, four examples have been carried out and the results are compared with standard FEM, the p-Fourier Method and analytical solutions.

In another paper, a closed-form dynamic stiffness (DS) formulation is proposed for exact transverse free vibration analysis of tapered and/or functionally graded beams based on Euler–Bernoulli theory [20]. Among the important points of this work is focusing on both the DS formulation and the solution technique. The authors point out that their work innovations can be effective in making exact and highly efficient modal analysis possible for a wide range of tapered and/or functionally graded beams, without resorting to series solution, numerical integrations or refined mesh discretization. They have also shown by their method that the results

for a particular case show excellent correspondence with the published results.

Banerjee and Ananthapuvirajah [21] have proposed an accurate dynamic stiffness matrix for a beam by integrating Rayleigh-Love theory for longitudinal vibration into Timoshenko theory for bending vibration. In this work in the formulation, Rayleigh-Love theory considers transvers inertia in longitudinal vibration, while Timoshenko beam theory considers the effects of shear deformation and rotating inertia in bending vibration. Then the dynamic stiffness matrix has been developed by solving the governing differential Equations of motion in free vibration of a Rayleigh-Love bar and a Timoshenko beam and imposing the boundary conditions for displacements and forces. Next two dynamic stiffness theories are combined using a unified notation. Also some of the computed results for some elements as a case study by this method have been compared with published ones.

All of the above research points to the importance of having the exact frequencies, shape functions and achieve more accurate dynamic analysis of one or more elements. In this research, we are going to achieve a more accurate frequency of this element by using the real shape functions of simple beams, and mass and stiffness matrices.

**2 INTRODUCING MASS AND STIFFNESS MATRICES OF BERNOULLI BEAM USING CLASSICAL SHAPE FUNCTIONS**

In this section, we introduce the classical shape functions of a Bernoulli beam obtained using the Bernoulli principle of “Eq. (1)”. Then, the classical mass and stiffness matrices are obtained using the classical shape functions and the concepts of kinetic, strain, and flexural energy.

$$EI.y(x)^{(IV)} = p(x) \tag{1}$$

In this study, we do not consider the effect of stability. In other words, the properties of buckling and stability are not considered on the element’s stiffness. This assumption is because the high-frequency elements considered in this study are that of the mass effect on these elements and are negligible compared to their stiffness, knowing that it is the mass that causes buckling in the elements. Therefore, we put  $(P(x) = 0)$  in “Eq. (1)”.

In the following, the classical shape functions of the Bernoulli beam are obtained using “Eq. (1)”. Figure 1 shows the six shape functions of the axial, across, and rotational motions of this beam.

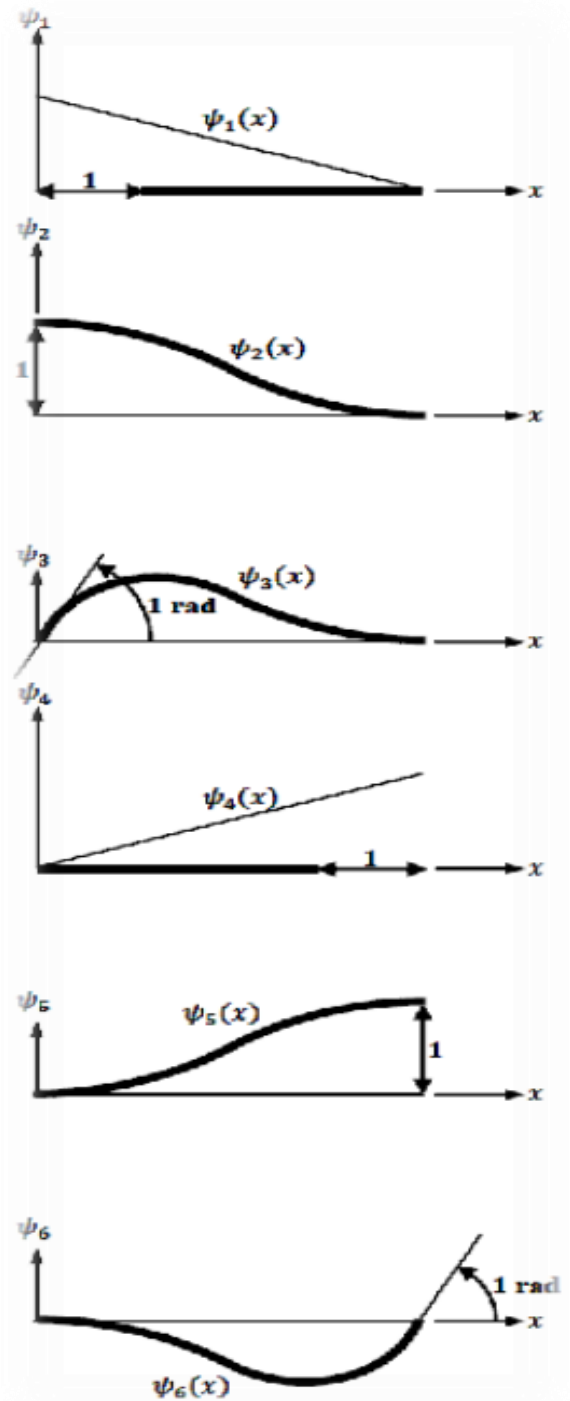


Fig. 1 Shape modes of a Bernoulli beam element.

$$\psi_{1\text{Classic}}(x) = 1 - \frac{1}{L} \cdot x \cdot d_1 \tag{2}$$

$$\psi_{2\text{Classic}}(x) = 1 - \frac{3}{L^2} \cdot x^2 + \frac{2}{L^3} \cdot x^3 \cdot d_2 \tag{3}$$

$$\psi_{3\text{Classic}}(x) = x - \frac{2}{L} \cdot x^2 + \frac{1}{L^2} \cdot x^3 \quad d_3 \quad (4)$$

$$\psi_{4\text{Classic}}(x) = \frac{1}{L} \cdot x \quad d_4 \quad (5)$$

$$\psi_{5\text{Classic}}(x) = \frac{3}{L^2} \cdot x^2 - \frac{2}{L^3} \cdot x^3 \quad d_5 \quad (6)$$

$$\psi_{6\text{Classic}}(x) = \frac{1}{L^2} \cdot x^3 - \frac{1}{L} \cdot x^2 \quad d_6 \quad (7)$$

**2.1. Classic Mass Matrix for Bernoulli Beam**

By putting in the axial shape functions ( $\psi_1$  and  $\psi_2$ ) of “Eqs. (2) and (5)” in relation to the axial kinetic energy, Eq. (8), the axial quantities of the classical mass matrix are formed.

$$m_{ij} = \int_0^L m \cdot \psi_i(x) \cdot \psi_j(x) dx \quad i, j = (1, 2, 3, 4, 5, 6) \quad (8)$$

For example:

$$m_{11\text{Classic}} = \quad (9)$$

$$\int_0^L m \cdot \psi_{1\text{Classic}}(x) \cdot \psi_{1\text{Classic}}(x) dx = \int_0^L m \cdot \left(1 - \frac{1}{L} \cdot x\right) \cdot \left(1 - \frac{1}{L} \cdot x\right) dx = \frac{mL}{3} \quad (10)$$

$$m_{44\text{Classic}} = m_{44\text{Classic}} =$$

$$\int_0^L m \cdot \psi_{4\text{Classic}}(x) \cdot \psi_{4\text{Classic}}(x) dx = \int_0^L m \cdot \left(\frac{1}{L} \cdot x\right) \cdot \left(\frac{1}{L} \cdot x\right) dx = \frac{mL}{6}$$

By putting in the across and rotational shape functions ( $\psi_2, \psi_3, \psi_5$  and  $\psi_6$ ) of “Eqs. (3), (4), (6) and (7)” in “Eq. (8)”, the lateral quantities of the classical mass matrix are created.

For example:

$$m_{22\text{Classic}} = m_{55\text{Classic}} = \quad (11)$$

$$\int_0^L m \cdot \psi_{2\text{Classic}}(x) \cdot \psi_{2\text{Classic}}(x) dx = \int_0^L m \cdot \left(1 - \frac{3}{L^2} \cdot x^2 + \frac{2}{L^3} \cdot x^3\right) \cdot \left(1 - \frac{3}{L^2} \cdot x^2 + \frac{2}{L^3} \cdot x^3\right) dx = \frac{13 \cdot mL}{35} \quad (12)$$

$$m_{23\text{Classic}} = m_{32\text{Classic}} =$$

$$\int_0^L m \cdot \psi_{2\text{Classic}}(x) \cdot \psi_{3\text{Classic}}(x) dx = \int_0^L m \cdot \left(1 - \frac{3}{L^2} \cdot x^2 + \frac{2}{L^3} \cdot x^3\right) \cdot \left(x - \frac{2}{L} \cdot x^2 + \frac{1}{L^2} \cdot x^3\right) dx = \frac{11 \cdot mL}{210}$$

**2.2. Classic Stiffness Matrix for Bernoulli Beam**

The axial values of the stiffness matrix are obtained as follows from the axial strain energy “Eq. (13)”.

$$k_{ij} = \int_0^L EA \cdot \psi'_i(x) \cdot \psi'_j(x) dx \quad (13)$$

$i, j = (1, 4)$

By deriving  $\psi_{1\text{Classic}}$  and  $\psi_{4\text{Classic}}$  of “Eqs. (2) and (5)” and placing them in the “Eq. (13)”, the axial quantities of the classical stiffness matrix are formed.

Then by applying the bending strain energy relation below (14) and placing the second-order derivatives of the classical shape functions in it, the lateral quantities of the classical stiffness matrix are formed.

$$k_{ij} = \int_0^L EI \cdot \psi''_i(x) \cdot \psi''_j(x) dx \quad i, j = (2, 3, 5, 6) \quad (14)$$

For example:

$$k_{22\text{Classic}} = \int_0^L EI \cdot \psi''_{2\text{Classic}}(x) \cdot \psi''_{2\text{Classic}}(x) dx = \int_0^L EI \cdot \left(-\frac{6}{L^2} + \frac{12}{L^3} \cdot x\right) \cdot \left(-\frac{6}{L^2} + \frac{12}{L^3} \cdot x\right) dx \quad (15)$$

**3 METHOD OF OBTAINING MASS AND STIFFNESS MATRICES OF BERNOULLI BEAM USING REAL SHAPE FUNCTIONS**

In this section, first, the Bernoulli beam lateral motion Equation is formulated using Newton’s second law, then, by solving this Equation and applying boundary conditions we obtain the real shape functions. Next, we obtain the mass and stiffness matrices of the beam using those real shape functions.

**3.1. Formulation of the Beam Motion Equation by Newton’s Second Law**

Figure 2 shows the free body diagram of a beam in length ( $dx$ ) and Newton’s second law for dynamic equilibrium forces.

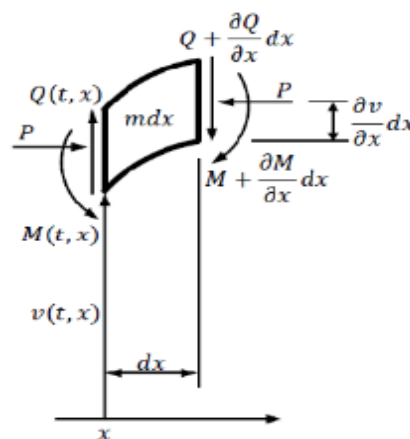


Fig. 2 Free body diagram of a beam (Newton’s second law).

Newton’s second law for forces dynamic equilibrium (With axial force):

$$m \cdot a = \sum_{i=1}^n F_i \quad (16)$$

We draw from “Eq. (16)”:

$$m \cdot \frac{\delta^2 v(t, x)}{\delta t^2} = -\frac{\delta Q}{\delta x} \quad (17)$$

Newton’s second law for Moments static equilibrium:

$$\sum_{i=1}^n M_i + \sum_{i=1}^n F_i \times r_i = 0 \quad (18)$$

By placing the beam moments in “Eq. (18)” and simplifying and applying “Eq. (17)”, the quadratic Equation of lateral motion of the beam is formed as follows:

$$\frac{\delta^2 v(t, x)}{\eta^2 \cdot \delta t^2} + \frac{\delta^4 v(t, x)}{\delta x^4} + \lambda^2 \cdot \frac{\delta^2 v(t, x)}{\delta x^2} = 0 \quad (19)$$

In the above Equation, the definitions of  $\eta^2$  and  $\lambda^2$  are:

$$\eta^2 = \frac{EI}{m} \quad \text{and} \quad \lambda^2 = \frac{P}{EI} \quad (20)$$

### 3.2. Method of Solving the Beam Lateral Motion Equation

To solve the beam motion Equation, we use the separation method.

$$v(t, x) = T(t) \cdot Y(x) \quad (21)$$

So, by applying the separation method to Eq. (19), we solve it as follows:

$$\frac{\delta^2 v(t, x)}{\delta t^2} = \frac{d^2 T(t)}{dt^2} \cdot Y(x) = T''(t) \cdot Y(x) \quad (22)$$

$$\frac{\delta^2 v(t, x)}{\delta x^4} = T(t) \cdot \frac{d^2 Y(x)}{dx^2} = T(t) \cdot Y''(x) \quad (23)$$

$$\frac{\delta^4 v(t, x)}{\delta x^4} = T(t) \cdot \frac{d^4 Y(x)}{dx^4} = T(t) \cdot Y''''(x) \quad (24)$$

Equations (22), (23) and (24) are placed into “Eq. (19)” and then separated into the displacement-dependent and time-dependent Equations, and each placed on the side of equality. Then, the two sides of the Equation are divided into  $Y(x)$  and make the whole Equation equal to

$\beta^4$ . Now, according to the above explanations, the Equation is transformed as follows:

$$\frac{Y''''(x)}{Y(x)} + \lambda^2 \cdot \frac{Y''(x)}{Y(x)} = -\frac{T''(t)}{\eta^2 T(t)} = \beta^4 \quad (25)$$

From “Eq. (25)”, we come to two displacement and time dependent differential Equations.

Time-dependent differential Equation:

$$\frac{d^2 T(t)}{dt^2} + \eta^2 \cdot \beta^4 \cdot T(t) = 0 \quad (26)$$

Displacement-dependent differential Equation:

$$Y''''(x) + \lambda^2 \cdot Y''(x) - \beta^4 \cdot Y(x) = 0 \quad (27)$$

By obtaining the roots of the displacement-dependent Equation, we arrive at the real shape functions. Since we do not consider the effect of stability in this study as explained in part two, that is  $P = 0$ , the result will be  $\lambda = 0$  with respect to “Eq. (20)”.

$$r^4 + \lambda^2 \cdot r^2 - \beta^4 = 0 \quad (28)$$

$$r_1 = \sqrt{\frac{\sqrt{\lambda^4 + 4 \cdot \beta^4} - \lambda^2}{2}} = \mu \quad (29)$$

$$r_2 = -\sqrt{\frac{\sqrt{\lambda^4 + 4 \cdot \beta^4} - \lambda^2}{2}} = -\mu \quad (30)$$

$$r_3 = i \sqrt{\frac{\sqrt{\lambda^4 + 4 \cdot \beta^4} + \lambda^2}{2}} = ik \quad (31)$$

$$r_4 = -i \sqrt{\frac{\sqrt{\lambda^4 + 4 \cdot \beta^4} + \lambda^2}{2}} = -ik \quad (32)$$

The obtained roots of the displacement-dependent differential Equation include two real roots of sines and hyperbolic cosines and two imaginary roots of the sines and cosines.

As a result, the real shape function of the beam is:

$$Y(x) = A \cdot \cos(kx) + B \cdot \sin(kx) + C \cdot \cosh(\mu x) + D \cdot \sinh(\mu x) \quad (33)$$

$$Y'(x) = -A \cdot k \cdot \sin(kx) + B \cdot k \cdot \cos(kx) + C \cdot \mu \cdot \sinh(\mu x) + D \cdot \mu \cdot \cosh(\mu x) \quad (34)$$

And we can say that ( $k = \mu = \beta$ ), so we have:

$$\psi_{\text{Real}}(x) = A.\cos(\beta x) + B.\sin(\beta x) + C.\cosh(\beta x) + D.\sinh(\beta x) \tag{35}$$

$$\psi'_{\text{Real}}(x) = -A.k.\sin(\beta x) + B.k.\cos(\beta x) + C.\mu.\sinh(\beta x) + D.\mu.\cosh(\beta x) \tag{36}$$

### 3.3. Applying Boundary Conditions and Obtaining Coefficients of Real Shape Functions

By applying boundary conditions and placing in the Equation of the real shape function achieved in the previous section, the coefficients of the real shape functions will be obtained. According to “Fig. 1” which shows the displacements and rotations under the unit load and unit moment at the beginning and the end of the element with ( $d_1, d_2, \dots$ , and  $d_6$ ), we have:

$$\psi_{\text{Real}}(x = 0) = d_2 \quad A + C = d_2 \tag{37}$$

$$\psi'_{\text{Real}}(x = 0) = d_3 \quad \beta \cdot (B + D) = d_3 \tag{38}$$

$$\psi_{\text{Real}}(x = L) = d_5 \quad A.\cos(\beta L) + B.\sin(\beta L) + C.\cosh(\beta L) + D.\sinh(\beta L) = d_5 \tag{39}$$

$$\psi'_{\text{Real}}(x = L) = d_6 \quad \beta \cdot (-A.\sin(\beta L) + B.\cos(\beta L) + C.\sinh(\beta L) + D.\cosh(\beta L)) = d_6 \tag{40}$$

Using the McLaurin expansion as well as the usual mathematical simplification, the coefficients of the second mode shape function are obtained as follows:

$$\psi_2 = \left(\frac{420 - 13\alpha^4}{176400}\right) \cdot \alpha^4 \cdot \left(\frac{x}{L}\right)^7 + \left(\frac{11\alpha^4 - 1260}{151200}\right) \cdot \alpha^4 \cdot \left(\frac{x}{L}\right)^6 + \frac{\alpha^4}{24} \cdot \left(\frac{x}{L}\right)^4 + \left(2 - \frac{13}{210} \cdot \alpha^4\right) \cdot \left(\frac{x}{L}\right)^3 + \left(\frac{11}{420} \cdot \alpha^4 - 3\right) \cdot \left(\frac{x}{L}\right)^2 + 1 \tag{44}$$

$$\beta = \sqrt{\frac{m}{EI}} \cdot \omega \quad \beta L = \alpha$$

The rest of the real shape functions are obtained as above.

### 3.4. Formation of Real Mass and Stiffness Matrices of Bernoulli Beam

As shown in the preceding section, the real shape functions depend on the natural frequency value of each element ( $\alpha$  and  $\beta$ ). Therefore, the mass and stiffness matrices of each element vary according to the natural

$$\begin{pmatrix} 1 & 0 & 1 & 0 \\ 0 & \beta & 0 & \beta \\ \cos(\beta.L) & \sin(\beta.L) & \cosh(\beta.L) & \sinh(\beta.L) \\ -\beta.\sin(\beta.L) & \beta.\cos(\beta.L) & \beta.\sinh(\beta.L) & \beta.\cosh(\beta.L) \end{pmatrix} \begin{pmatrix} A \\ B \\ C \\ D \end{pmatrix} = \begin{pmatrix} d_2 \\ d_3 \\ d_5 \\ d_6 \end{pmatrix} \tag{41}$$

As an example, for the second mode shape, we set ( $d_2 = 1$ ) and ( $d_3, d_5, d_6 = 0$ ) into (41). Then, we obtain the coefficients and, thereafter, the real shape functions of the second mode are as follows:

By definition ( $\beta L = \alpha$ ) we have:

$$\begin{pmatrix} A \\ B \\ C \\ D \end{pmatrix} \psi_{2\text{Real}} = \begin{pmatrix} \frac{-1}{2} \cdot \frac{(1 + \sin(\alpha) \cdot \sinh(\alpha) - \cos(\alpha) \cdot \cosh(\alpha))}{(\cos(\alpha) \cdot \cosh(\alpha) - 1)} \\ \frac{1}{2} \cdot \frac{(\cos(\alpha) \cdot \sinh(\alpha) + \sin(\alpha) \cdot \cosh(\alpha))}{(\cos(\alpha) \cdot \cosh(\alpha) - 1)} \\ \frac{1}{2} \cdot \frac{(\cos(\alpha) \cdot \cosh(\alpha) + \sin(\alpha) \cdot \sinh(\alpha) - 1)}{(\cos(\alpha) \cdot \cosh(\alpha) - 1)} \\ \frac{-1}{2} \cdot \frac{(\cos(\alpha) \cdot \sinh(\alpha) + \sin(\alpha) \cdot \cosh(\alpha))}{(\cos(\alpha) \cdot \cosh(\alpha) - 1)} \end{pmatrix} \tag{42}$$

By placing the coefficients obtained from the above relation into the real shape function, “Eq. (35)”, the real shape function of the second mode is created as follows.

$$\psi_{2\text{Real}} = (\cos(\beta x) \sin(\beta x) \cosh(\beta x) \sinh(\beta x)) \cdot \begin{pmatrix} \frac{-1}{2} \cdot \frac{(1 + \sin(\alpha) \cdot \sinh(\alpha) - \cos(\alpha) \cdot \cosh(\alpha))}{(\cos(\alpha) \cdot \cosh(\alpha) - 1)} \\ \frac{1}{2} \cdot \frac{(\cos(\alpha) \cdot \sinh(\alpha) + \sin(\alpha) \cdot \cosh(\alpha))}{(\cos(\alpha) \cdot \cosh(\alpha) - 1)} \\ \frac{1}{2} \cdot \frac{(\cos(\alpha) \cdot \cosh(\alpha) + \sin(\alpha) \cdot \sinh(\alpha) - 1)}{(\cos(\alpha) \cdot \cosh(\alpha) - 1)} \\ \frac{-1}{2} \cdot \frac{(\cos(\alpha) \cdot \sinh(\alpha) + \sin(\alpha) \cdot \cosh(\alpha))}{(\cos(\alpha) \cdot \cosh(\alpha) - 1)} \end{pmatrix} \tag{43}$$

frequency value of that element, and to obtain real and total mass and stiffness matrices of a frame or structure, one must obtain the mass and stiffness matrices of each assembled element.

The real mass matrix using “Eq. (8)” is:

$$m_{\text{Real}} = m \cdot \begin{pmatrix} \frac{L}{3} & 0 & 0 & \frac{L}{6} & 0 & 0 \\ 0 & \int_0^L \psi_{2\text{Real}} \cdot \psi_{2\text{Real}} dx & \int_0^L \psi_{2\text{Real}} \cdot \psi_{3\text{Real}} dx & 0 & \int_0^L \psi_{2\text{Real}} \cdot \psi_{5\text{Real}} dx & \int_0^L \psi_{2\text{Real}} \cdot \psi_{6\text{Real}} dx \\ 0 & \int_0^L \psi_{3\text{Real}} \cdot \psi_{2\text{Real}} dx & \int_0^L \psi_{3\text{Real}} \cdot \psi_{3\text{Real}} dx & 0 & \int_0^L \psi_{3\text{Real}} \cdot \psi_{5\text{Real}} dx & \int_0^L \psi_{3\text{Real}} \cdot \psi_{6\text{Real}} dx \\ \frac{L}{6} & 0 & 0 & \frac{L}{3} & 0 & 0 \\ 0 & \int_0^L \psi_{5\text{Real}} \cdot \psi_{2\text{Real}} dx & \int_0^L \psi_{5\text{Real}} \cdot \psi_{3\text{Real}} dx & 0 & \int_0^L \psi_{5\text{Real}} \cdot \psi_{5\text{Real}} dx & \int_0^L \psi_{5\text{Real}} \cdot \psi_{6\text{Real}} dx \\ 0 & \int_0^L \psi_{6\text{Real}} \cdot \psi_{2\text{Real}} dx & \int_0^L \psi_{6\text{Real}} \cdot \psi_{3\text{Real}} dx & 0 & \int_0^L \psi_{6\text{Real}} \cdot \psi_{5\text{Real}} dx & \int_0^L \psi_{6\text{Real}} \cdot \psi_{6\text{Real}} dx \end{pmatrix} \quad (45)$$

The real stiffness matrix using “Eq. (14)” is:

$$k_{\text{Real}} = m \cdot \begin{pmatrix} \frac{A}{IL} & 0 & 0 & -\frac{A}{IL} & 0 & 0 \\ 0 & \int_0^L \psi''_{2\text{Real}} \cdot \psi''_{2\text{Real}} dx & \int_0^L \psi''_{2\text{Real}} \cdot \psi''_{3\text{Real}} dx & 0 & \int_0^L \psi''_{2\text{Real}} \cdot \psi''_{5\text{Real}} dx & \int_0^L \psi''_{2\text{Real}} \cdot \psi''_{6\text{Real}} dx \\ 0 & \int_0^L \psi''_{3\text{Real}} \cdot \psi''_{2\text{Real}} dx & \int_0^L \psi''_{3\text{Real}} \cdot \psi''_{3\text{Real}} dx & 0 & \int_0^L \psi''_{3\text{Real}} \cdot \psi''_{5\text{Real}} dx & \int_0^L \psi''_{3\text{Real}} \cdot \psi''_{6\text{Real}} dx \\ -\frac{A}{IL} & 0 & 0 & \frac{A}{IL} & 0 & 0 \\ 0 & \int_0^L \psi''_{5\text{Real}} \cdot \psi''_{2\text{Real}} dx & \int_0^L \psi''_{5\text{Real}} \cdot \psi''_{3\text{Real}} dx & 0 & \int_0^L \psi''_{5\text{Real}} \cdot \psi''_{5\text{Real}} dx & \int_0^L \psi''_{5\text{Real}} \cdot \psi''_{6\text{Real}} dx \\ 0 & \int_0^L \psi''_{6\text{Real}} \cdot \psi''_{2\text{Real}} dx & \int_0^L \psi''_{6\text{Real}} \cdot \psi''_{3\text{Real}} dx & 0 & \int_0^L \psi''_{6\text{Real}} \cdot \psi''_{5\text{Real}} dx & \int_0^L \psi''_{6\text{Real}} \cdot \psi''_{6\text{Real}} dx \end{pmatrix} \quad (46)$$

#### 4 CASE STUDIES ON THE ACCURACY OF THE NATURAL FREQUENCY VALUE OBTAINED USING CLASSICAL AND REAL MASS AND STIFFNESS MATRICES

In this section, we obtain simple beam natural frequency with eigenvalue analysis for different support conditions with classical and real mass and stiffness matrices. To do this, we first obtain initial frequency from classical mass and stiffness matrices by eigenvalue analysis and compare it to the exact frequency. Then, we make the shape functions and the real mass and stiffness matrices using the initial frequency, and obtain the frequency of the real shape functions by eigenvalue analysis, and accurately compare this with the exact frequency and frequency values obtained from classical shape functions. The MATHCAD 2000 software was used for the calculations.

##### a. Simply-Supported beam

In the following relationship the exact value of the natural frequency of the first mode for this beam is shown, which is obtained from the characteristic Equation method [22].

$$\omega_{\text{exact}}(\text{main mode})_{\text{s-s}} = \pi^2 \cdot \sqrt{\frac{EI}{m \cdot L^4}} \quad (47)$$

The simply-supported beam has three degrees of freedom. (“Fig. 3”)

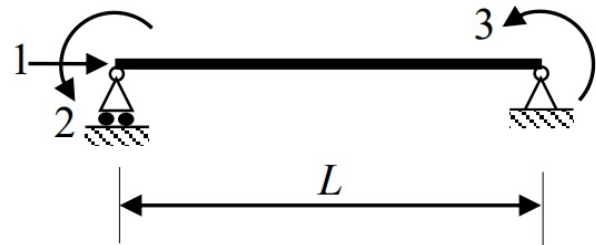


Fig. 3 The degree of freedom of simply supported beam.

We obtain the mass and stiffness matrices of this beam by forming the MCM and transfer matrices, and by pre-multiplying and post-multiplying the T matrix by the classical mass and stiffness matrices. MCM and transfer matrices are formed for simply-supported beam below.

$$T = \begin{pmatrix} 1 & 0 & 0 \\ 0 & 0 & 0 \\ 0 & 1 & 0 \\ 0 & 0 & 0 \\ 0 & 0 & 0 \\ 0 & 0 & 1 \end{pmatrix} MCM = \begin{pmatrix} 1 \\ 0 \\ 2 \\ 0 \\ 0 \\ 3 \end{pmatrix} \quad (48)$$

Classic mass matrix of simply- supported beam:

$$T^T \cdot mL \cdot \begin{pmatrix} \frac{1}{3} & 0 & 0 & \frac{1}{6} & 0 & 0 \\ 0 & \frac{13}{35} & \frac{11}{210} \cdot L & 0 & \frac{9}{70} & \frac{-13}{420} \cdot L \\ 0 & \frac{11}{210} \cdot L & \frac{1}{105} \cdot L^2 & 0 & \frac{13}{420} \cdot L & \frac{-1}{140} \cdot L^2 \\ \frac{1}{6} & 0 & 0 & \frac{1}{3} & 0 & 0 \\ 0 & \frac{9}{70} & \frac{13}{420} \cdot L & 0 & \frac{13}{35} & \frac{-11}{210} \cdot L \\ 0 & \frac{-13}{420} \cdot L & \frac{-1}{140} \cdot L^2 & 0 & \frac{-11}{210} \cdot L & \frac{1}{105} \cdot L^2 \end{pmatrix} \cdot T \rightarrow \quad (49)$$

$$m_{\text{Classic(s-s)}} = \begin{pmatrix} \frac{1}{3} \cdot mL & 0 & 0 \\ 0 & \frac{1}{105} \cdot mL \cdot L^2 & \frac{-1}{140} \cdot mL \cdot L^2 \\ 0 & \frac{-1}{140} \cdot mL \cdot L^2 & \frac{1}{105} \cdot mL \cdot L^2 \end{pmatrix}$$

Classic stiffness matrix of simply- supported beam:

$$T^T \cdot \begin{pmatrix} \frac{EA}{L} & 0 & 0 & \frac{EA}{L} & 0 & 0 \\ 0 & \frac{12 \cdot EI}{L^3} & \frac{6 \cdot EI}{L^2} & 0 & \frac{12 \cdot EI}{L^3} & \frac{6 \cdot EI}{L^2} \\ 0 & \frac{6 \cdot EI}{L^2} & \frac{4 \cdot EI}{L} & 0 & \frac{6 \cdot EI}{L^2} & \frac{2 \cdot EI}{L} \\ -\frac{EA}{L} & 0 & 0 & \frac{EA}{L} & 0 & 0 \\ 0 & -\frac{12 \cdot EI}{L^3} & -\frac{6 \cdot EI}{L^2} & 0 & \frac{12 \cdot EI}{L^3} & \frac{6 \cdot EI}{L^2} \\ 0 & \frac{6 \cdot EI}{L^2} & \frac{2 \cdot EI}{L} & 0 & -\frac{6 \cdot EI}{L^2} & \frac{4 \cdot EI}{L} \end{pmatrix} \cdot T \rightarrow \quad (50)$$

$$k_{\text{Classic(s-s)}} = \begin{pmatrix} \frac{EA}{L} & 0 & 0 \\ 0 & 4 \cdot \frac{EI}{L} & 2 \cdot \frac{EI}{L} \\ 0 & 2 \cdot \frac{EI}{L} & 4 \cdot \frac{EI}{L} \end{pmatrix}$$

Eigenvalue analysis:

$$\left| K - \omega^2 \cdot M \right| = 0 \quad \omega^2 = s \quad (51)$$

$$\begin{pmatrix} \frac{EA}{L} & 0 & 0 \\ 0 & 4 \cdot \frac{EI}{L} & 2 \cdot \frac{EI}{L} \\ 0 & 2 \cdot \frac{EI}{L} & 4 \cdot \frac{EI}{L} \end{pmatrix} - s \cdot \begin{pmatrix} \frac{1}{3} \cdot mL & 0 & 0 \\ 0 & \frac{1}{105} \cdot mL \cdot L^2 & \frac{-1}{140} \cdot mL \cdot L^2 \\ 0 & \frac{-1}{140} \cdot mL \cdot L^2 & \frac{1}{105} \cdot mL \cdot L^2 \end{pmatrix} \text{ solve, } s = \quad (52)$$

$$\omega^2_{\text{Classic(s-s)}} = \begin{bmatrix} 3 \cdot \frac{EA}{(mL \cdot L)} \\ 120 \cdot \frac{EI}{(mL \cdot L^3)} \\ 2520 \cdot \frac{EI}{(mL \cdot L^3)} \end{bmatrix}$$

We obtained the eigenvalues for this beam using the classical matrices above. The first quantity in “Eq. (52)” relates to the degree of axial freedom that we do not consider. So, our second quantity in this matrix is the first eigenvalue and it is the main mode.

By extracting the square root of the eigenvalue, we arrive at the natural frequency. Comparing the exact frequency value of “Eq. (47)” and the root of the “Eq. (52)” below, we obtain the value of the frequency error obtained by the classical method.

$$\omega_{(\text{main mode})_{\text{Classic(s-s)}}} = \sqrt{120 \frac{EI}{mL^4}} \neq \omega_R = \pi^2 \sqrt{\frac{EI}{mL^4}} \rightarrow \sqrt{120} = 10.954 \neq \pi^2 \quad (53)$$

Percentage of frequency error of the main mode by the classical method compared to the exact value (47):

$$e_{\text{Classic(s-s)}} = \frac{10.954 - \pi^2}{\pi^2} = 10.987\% \quad (54)$$

Now, using the real mass and stiffness matrix (45) and (46) and like the method we used to obtain the classic system matrix mode above, we obtain the real mass and stiffness matrices of this beam. The value of  $\alpha$ , to apply to real shape functions, and the real mass and stiffness matrix for the beam mentioned above is obtained by the following relations:

$$\text{We had } \beta = \sqrt{\frac{m}{EI}} \cdot \omega \quad \text{and} \quad \alpha = \beta L$$

Real mass matrix of simply- supported beam using the real mass matrix (45):

$$m_{\text{Real(s-s)}} = T^T m_{\text{Real}} T = \begin{bmatrix} \frac{1}{3} \cdot L \cdot m & 0 & 0 \\ 0 & 0.015 \cdot L^3 \cdot m & -0.013 \cdot L^3 \cdot m \\ 0 & -0.013 \cdot L^3 \cdot m & 0.015 \cdot L^3 \cdot m \end{bmatrix} \quad (58)$$

Real stiffness matrix of simply- supported beam using the real stiffness matrix (46):

$$k_{\text{Real(s-s)}} = T^T k_{\text{Real}} T = \begin{bmatrix} \frac{EA}{L} & 0 & 0 \\ 0 & \frac{4.402}{L} \cdot EI & \frac{1.605}{L} \cdot EI \\ 0 & \frac{1.605}{L} \cdot EI & \frac{4.402}{L} \cdot EI \end{bmatrix} \quad (59)$$

The eigenvalues are obtained by “Eq. (50)”:

$$\omega^2_{\text{Real(s-s)}} = \begin{bmatrix} 3 \cdot A \cdot \frac{EI}{(L^2 \cdot m \cdot l)} \\ 98.649 \cdot \frac{EI}{(m \cdot L^4)} \\ 2382.888 \cdot \frac{EI}{(m \cdot L^4)} \end{bmatrix} \quad (60)$$

We obtained the eigenvalues for this beam using the real matrices above. The first quantity in “Eq. (60)” relates to the degree of axial freedom that we do not consider. So, our second quantity in this matrix is the first eigenvalue and it is the main mode.

Natural frequency of the main mode of beam using the real mass and stiffness matrices:

$$\omega_{\text{main mode}}_{\text{Real(s-s)}} = \sqrt{98.649 \cdot \frac{EI}{(m \cdot L^4)}} = 9.932 \sqrt{\frac{EI}{m \cdot L^4}} \quad (61)$$

Comparing the frequency value obtained, using the real shape functions above, with the exact value of the natural frequency of this beam, that is, “Eq. (47)” the percentage of frequency error of the main mode is obtained.

$$e_{\text{Real(s-s)}} = \frac{9.932 - \pi^2}{\pi^2} = 0.632\% \quad (62)$$

### b. Clamped (Fixed - Ended) Beam

The only difference for this beam is that it cannot be solved by considering it as an element because it lacks any degree of freedom; therefore, as shown in “Fig. 4”, we divide this beam in two equal parts  $L/2$  in length.

Now, each part has three degrees of freedom. So, we have a transfer, mass and stiffness matrices, for each part of the beam. In order to obtain the mass and stiffness matrices of the whole beam in classical and real state,

we must assemble the mass and stiffness matrices obtained from the two parts of the beam that were formed using the transfer matrix of each part.

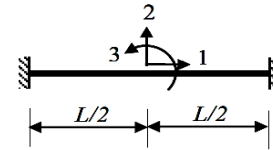


Fig. 4 The degree of freedom of fixed - ended beam.

For the remaining steps in case study (b), we follow the same procedure as in case study (a).

In the following, the exact value relationship is shown for the natural frequency of the main mode of this beam, which is obtained from the characteristic Equation method [22].

$$\omega_{\text{exact}}_{(\text{main - mode})\text{F-F}} = 22.373 \cdot \sqrt{\frac{EI}{m \cdot L^4}} \quad (63)$$

MCM and transfers matrices for this beam for each part of the beam the length of  $L/2$ :

$$MCM = \begin{pmatrix} 0 & 1 \\ 0 & 2 \\ 0 & 3 \\ 1 & 0 \\ 2 & 0 \\ 3 & 0 \end{pmatrix} T_{1(\text{for left } \frac{L}{2})} = \begin{pmatrix} 0 & 0 & 0 \\ 0 & 0 & 0 \\ 0 & 0 & 0 \\ 1 & 0 & 0 \\ 0 & 1 & 0 \\ 0 & 0 & 1 \end{pmatrix} \quad (64)$$

$$T_{2(\text{for right } \frac{L}{2})} = \begin{pmatrix} 1 & 0 & 0 \\ 0 & 1 & 0 \\ 0 & 0 & 1 \\ 0 & 0 & 0 \\ 0 & 0 & 0 \\ 0 & 0 & 0 \end{pmatrix}$$

Classic mass matrix of fixed-ended beam using the classic mass matrix:

$$m_{1 \text{ Classic(F-F)}} = \begin{pmatrix} \frac{1}{6} \cdot m \cdot L & 0 & 0 \\ 0 & \frac{13}{70} \cdot m \cdot L & \frac{-11}{840} \cdot m \cdot L^2 \\ 0 & \frac{-11}{840} \cdot m \cdot L^2 & \frac{1}{840} \cdot m \cdot L^3 \end{pmatrix}$$

$$m_{2 \text{ Classic(F-F)}} = \begin{pmatrix} \frac{1}{6} \cdot m \cdot L & 0 & 0 \\ 0 & \frac{13}{70} \cdot m \cdot L & \frac{11}{840} \cdot m \cdot L^2 \\ 0 & \frac{11}{840} \cdot m \cdot L^2 & \frac{1}{840} \cdot m \cdot L^3 \end{pmatrix} \quad (65)$$

$$m_{\text{Assembled (classic, F-F)}} = m_1 + m_2 = \begin{pmatrix} \frac{1}{3} \cdot m \cdot L & 0 & 0 \\ 0 & \frac{13}{35} \cdot m \cdot L & \frac{11}{840} \cdot m \cdot L^2 \\ 0 & 0 & \frac{1}{420} \cdot m \cdot L^3 \end{pmatrix}$$

$$m_{\text{Assembled (Real, F-F)}} = \begin{pmatrix} \frac{1}{3} \cdot m \cdot L & 0 & 0 \\ 0 & .397 \cdot m \cdot L & 3 \cdot 10^{-21} \cdot m \cdot L^2 \\ 0 & 3 \cdot 10^{-21} \cdot m \cdot L^2 & 2.67 \cdot 10^{-3} \cdot m \cdot L^3 \end{pmatrix} \quad (69)$$

Classic stiffness matrix of fixed-ended beam:

$$k_{\text{Assembled (classic, F-F)}} = \begin{pmatrix} 4 \cdot \frac{AE}{L} & 0 & 0 \\ 0 & 192 \cdot \frac{EI}{L^3} & 0 \\ 0 & 0 & 16 \frac{EI}{L} \end{pmatrix} \quad (66)$$

$$k_{\text{Assembled (Real, F-F)}} = \begin{pmatrix} 4 \cdot \frac{EA}{L} & 0 & 0 \\ 0 & 198.92 \cdot \frac{EI}{L^3} & 1 \cdot 10^{-18} \cdot \frac{EI}{L^2} \\ 0 & 1 \cdot 10^{-18} \cdot \frac{EI}{L^2} & 16.08 \frac{EI}{L} \end{pmatrix} \quad (70)$$

By Eigenvalue analysis:

$$\omega^2_{\text{Classic(F-F)}} = \begin{bmatrix} 12 \cdot \frac{EA}{m \cdot L^2} \\ 516.92 \cdot \frac{EI}{m \cdot L^4} \\ 6720 \cdot \frac{EI}{m \cdot L^4} \end{bmatrix} \quad (67)$$

By Eigenvalue analysis:

$$\omega^2_{\text{Real (F-F)}} = \begin{bmatrix} 12 \cdot \frac{EA}{m \cdot L^2} \\ 500.58 \cdot \frac{EI}{m \cdot L^4} \\ 6019.34 \cdot \frac{EI}{m \cdot L^4} \end{bmatrix} \quad (71)$$

$$\omega_{\text{main mode (F-F)classic}} = \sqrt{516.92 \frac{EI}{(m \cdot L^4)}} = 22.736 \sqrt{\frac{EI}{mL^4}}$$

$$\omega_{\text{main mode (F-F)Real}} = \sqrt{500.58 \frac{EI}{(m \cdot L^4)}} = 22.374 \sqrt{\frac{EI}{mL^4}}$$

Percentage of frequency error of the main mode from the value obtained by the classic method (67) compared to the exact value (63):

$$e_{\text{Classic(F-F)}} = \frac{22.736 - 22.373}{22.373} = 1.621\% \quad (68)$$

Percentage of frequency error of the main mode from the value obtained by the real method (71) compared to the exact value (63):

$$e_{\text{Real(F-F)}} = \frac{22.374 - 22.373}{22.373} = .002\% \quad (72)$$

The value of  $\alpha$  to put in matrices (45) and (46) and the real mass and stiffness formation matrices of this beam are obtained as described in case (a).

By putting the exact frequency value of the “Eq. (63)” into the “Eq. (55)” the value of  $\alpha$  is 4.77. Only half of the beam was considered in this case, thus, the value of  $\alpha$  is:

$$\alpha = \frac{4.77}{2} = 2.38$$

By pre-multiplying and post-multiplying, the T matrices (64) by the real mass and stiffness matrices, we obtain the mass and stiffness matrices of this beam. Real mass and stiffness matrices of fixed-fixed beam:

## 5 FINDINGS AND DISCUSSION

As observed, the coefficients and real shape functions, and consequently, the real mass and real stiffness matrices are obtained by solving the beam motion Equation. It is shown that the real shape functions are very different from the classic shape functions, so the mass and stiffness matrices obtained from them are also different. As shown in “Figs. 7 and 8”, the difference between classical and real shape functions is that the real shape functions are dependent on the element natural frequency ( $\alpha$  and  $\beta$ ) addition to the geometrical properties. In this paper, the beam element is considered and case studies are performed on two simple beams with different support conditions.

In both case studies, it was found that the accuracy of the natural frequency obtained using real shape functions is much higher than that of the natural frequency obtained using classical shape functions (“Table 1”). So, with this achievement we can obtain more accurate responses,

designs, analyses, and ultimately, better structural implementation against natural and human hazards by using more accurate natural frequencies in the dynamic analysis.

**Table 1** Comparison of natural frequency values obtained by classical and real shape functions with exact values for two case studies

Case	Exact value of natural frequency [21] (Main mode)	Natural frequency value by the classical method (Main mode)	Frequency error percentage by classical method	Natural frequency value by the real shape functions (Main mode)	Frequency error percentage by real shape functions (Main mode)
a. Simply-Supported beam	$\pi^2 \cdot \sqrt{\frac{EI}{m \cdot L^4}}$	$10.954 \cdot \sqrt{\frac{EI}{m \cdot L^4}}$	10.987%	$9.932 \cdot \sqrt{\frac{EI}{m \cdot L^4}}$	0.632%
b. Fixed-Fixed beam	$22.373 \cdot \sqrt{\frac{EI}{m \cdot L^4}}$	$22.74 \cdot \sqrt{\frac{EI}{m \cdot L^4}}$	1.621%	$22.374 \cdot \sqrt{\frac{EI}{m \cdot L^4}}$	.002%

In “Table 1”, for the two beams studied, the exact natural frequency value is compared with the natural frequencies obtained from the classical and real methods in the main mode. Also, the table presents the error values of the two methods.

Figures 5 and 6 show a noticeable reduction in the percentage of natural frequency error obtained by the two beams studied using the exact shape functions. Figures 7 and 8 present the dependence of the exact shape functions on the natural frequency of the elements. Overall, the higher the natural frequency of an element, the greater the difference between the exact and classical shape functions will be.



**Fig. 5** Frequency error percentage by classical method (main mode).

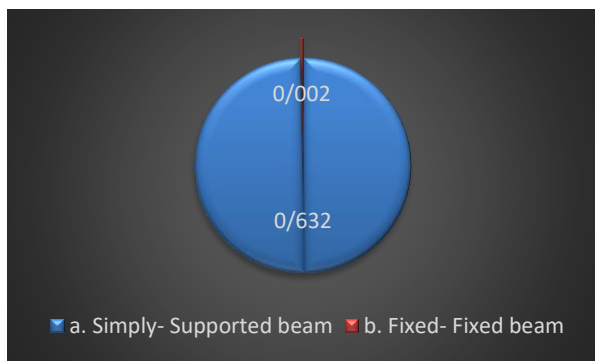


**Fig. 6** Frequency error percentage by real shape functions (main mode).

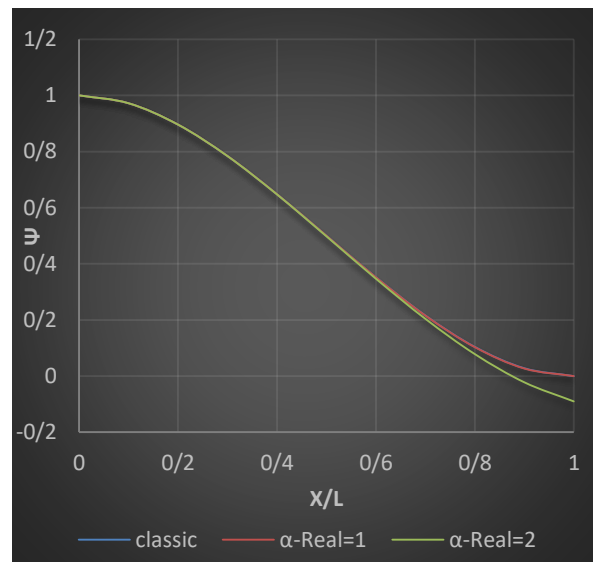


**Fig. 7** Comparison of the classic and real shape functions for the second mode with values ( $\alpha = \beta L = 1, 2, \beta = \sqrt{m/EI} \omega$ ), (At a value of  $\alpha = 1$ , the real shape function is located exactly on the classic shape function) -scaled length.

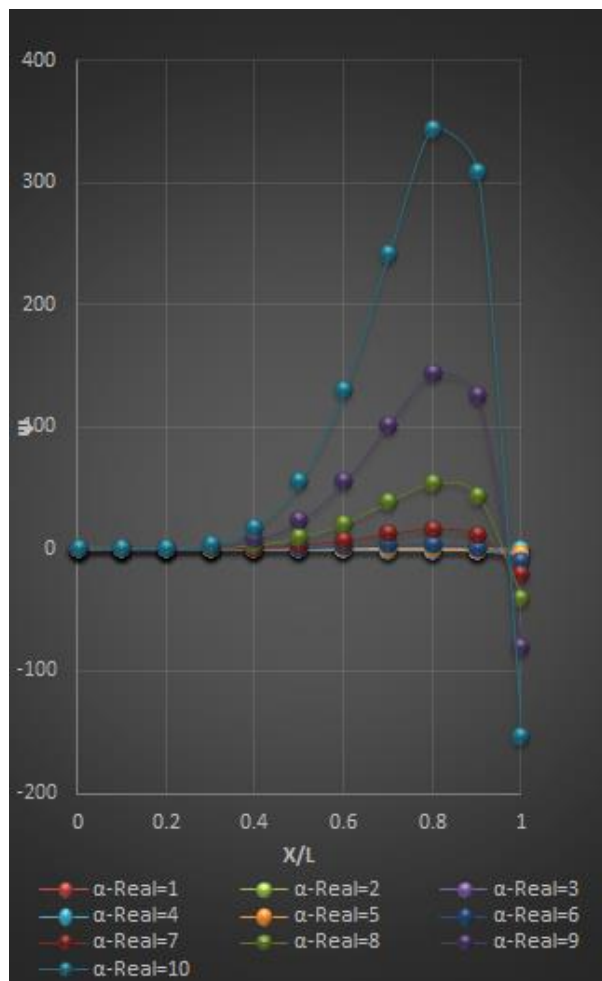


Fig. 8 Comparison of real shape functions for the second mode with different values of  $\alpha$  that depend on the natural frequency ( $\alpha = \beta L, \beta = \sqrt{m/EI} \omega$ )-scaled length.

## 6 CONCLUSIONS

1- As shown for the second mode shape functions (42) and (43), the coefficients of the real shape functions, and consequently, the real shape functions, become harmonic and hyperbolic. In contrast, the coefficients of the classical shape functions are simple.

2- Since the real shape functions depend on the natural frequency value of the element, the real mass and the real stiffness matrix of each element are also dependent on the element frequency. Therefore, to form a real mass and stiffness matrix of a total frame or structure, it is necessary to separately obtain each element's mass and stiffness matrices and then assemble them.

3- From the case studies of two simple beams in Section 4, we conclude that the main mode frequency error obtained by the real shape functions is approximately 0% ("Table 1, Figs. 5 and 6").

4- The frequency errors obtained by the classical method increase in elements with a higher natural frequency.

5- According to "Table 1", the frequency error percentage obtained using the real shape functions in the first case study is about 17 times lower than that obtained by the classical method. In the second case study, the frequency error percentage obtained using real shape functions is about 800 times lower than that obtained by the classical method.

6- According to "Table 1", the accuracy of the frequency value obtained by the real shape functions is high. As can be seen from this table, the case studies can achieve relatively accurate natural frequency by obtaining the actual shape functions of each element.

7- As can be seen, the real shape functions are seventh-degree. Since we have four boundary conditions, the remaining additional degrees are adjusted and satisfied according to the natural frequency of the system and the Bernoulli beam motion Equations ("Eq. 44"). For elements with a natural frequency close to 0, since  $\beta$  tends to 0 and consequently  $\alpha$  also tends to 0, the real shape functions will be the same as the classical shape functions, which means that the shape function the actual depends on the frequency value ("Figs. 7 and 8").

## REFERENCES

- [1] Rahbar, A., Abdollah, S., Free Vibrations of Reinforced Sheets of Sheep Structures, 17th Marine Industry Conference, Kish Island, Iranian Marine Engineering Association, 2015.
- [2] Azimi-Zawareie, S., Exact Dynamic Analysis of Truss Structures, Iranian Journal of International Institute of Seismology and Earthquake Engineering, No. 1, 1994.
- [3] Rana, H. K., Dynamic Analysis of Fixed-Fixed Beams, 2012.
- [4] Satpathy, S. M., Dash, P., Dynamic Analysis of Cantilever Beam and Its Experimental Validation, 2014.
- [5] Sawant, S., Experimental Verification of Transverse Vibration of Free-Free Beam, International Journal of Advanced Research in Electrical Electronics and Instrumentation Engineering, 2013.
- [6] Tatar, İ., Vibration Characteristics of Portal Frames, İzmir Institute of Technology, 2013.
- [7] AL, G., Kumawat, S. C., World Research Journal of Civil Engineering, 2011.
- [8] Chao, X., Dong, W., Experimental Investigation of Nonlinear Interface Effects in a Jointed Beam, Vibroengineering Procedia, Vol. 4, 2014, pp. 107-112.
- [9] Delhez, E., Experimental and Numerical Modal Analyses of a Pre-Stressed Steel Strip, ULiège-Université de Liège, 2017.
- [10] Esfandiari, A., Rahai, A., Sanayei, M., and Bakhtiari-Nejad, F., Model Updating of a Concrete Beam With

- Extensive Distributed Damage Using Experimental Frequency Response Function, *Journal of Bridge Engineering*, Vol. 21, No. 4, 2016, pp. 04015081.
- [11] Gandomkar, F., Wan Badaruzzaman, W., Osman, S., and Ismail, A., Experimental and Numerical Investigation of The Natural Frequencies of The Composite Profiled Steel Sheet Dry Board (PSSDB) System, *Journal of the South African Institution of Civil Engineering= Joernaal van die Suid-Afrikaanse Instituut van Siviele Ingenieurswese*, Vol. 55, No. 1, 2013, pp. 11-21.
- [12] Joubaneh, E. F., Barry, O. R., and Tanbour, H. E., Analytical and Experimental Vibration of Sandwich Beams Having Various Boundary Conditions, *Shock and Vibration*, Vol. 2018, 2018.
- [13] Krishnaraju, A., Ramkumar, R., and Lenin, V., Experimental Investigation of Natural Frequency of a Cantilever Composite Beam using Vibration Absorber, 2016.
- [14] Trišović, N., Eigenvalue Sensitivity Analysis in Structural Dynamics, *FME Transactions*, Vol. 35, No. 3, 2007, pp. 149-156.
- [15] Yang, C., Zhang, Z., Nong, S., and Zhu, C., Analytical and Experimental Investigation on Eigenfrequency-Based Damage Diagnosis of Cantilever Beam, *Journal of Vibroengineering*, Vol. 18, No. 8, 2016, pp. 5114-5126.
- [16] Chen, J., Bao, H., Wang, T., Desbrun, M., and Huang, J., Numerical Coarsening using Discontinuous Shape Functions, *ACM Transactions on Graphics (TOG)*, Vol. 37, No. 4, 2018, pp. 1-12.
- [17] Mousavi, Z., Eftefagh, M. M., Sadeghi, M. H., and Razavi, S. N., Developing Deep Neural Network for Damage Detection of Beam-Like Structures Using Dynamic Response Based on FE Model and Real Healthy State, *Applied Acoustics*, Vol. 168, 2020, pp. 107402.
- [18] Adhikari, S., Karličić, D., and Liu, X., Dynamic Stiffness of Nonlocal Damped Nano-Beams on Elastic Foundation, *European Journal of Mechanics-A/Solids*, Vol. 86, 2021, pp. 104144.
- [19] Corrêa, R. M., Arndt, M., and Machado, R. D., Free In-Plane Vibration Analysis of Curved Beams by The Generalized/Extended Finite Element Method, *European Journal of Mechanics-A/Solids*, Vol. 88, 2021, pp. 104244.
- [20] Liu, X., Chang, L., Banerjee, J. R., and Dan, H. C., Closed-Form Dynamic Stiffness Formulation for Exact Modal Analysis of Tapered and Functionally Graded Beams and Their Assemblies, *International Journal of Mechanical Sciences*, Vol. 214, 2022, pp. 106887.
- [21] Banerjee, J. R., Ananthapuvirajah, A., An Exact Dynamic Stiffness Matrix for a Beam Incorporating Rayleigh-Love and Timoshenko Theories, *International Journal of Mechanical Sciences*, Vol. 150, 2019, pp. 337-347.
- [22] Talukdar, S., *Vibration of Continuous Systems*, Professor, Department of Civil Engineering, Indian Institute of Technology Guwahati-781039, 2016.